# Stress field evolution above the Peruvian flat-slab (Cordillera Blanca, northern Peru)

A. Margirier[*], L. Audin, X. Robert, A. Pêcher, S. Schwartz

*Université Grenoble, Alpes, CNRS, IRD, ISTerre, F-38000 Grenoble, France*

## A B S T R A C T

In subduction settings, the tectonic regime of the overriding plate is closely related to the geometry of the subducting plate. Flat-slab segments are supposed to increase coupling at the plate interface in the Andes, resulting in an increase and eastward migration of the shortening in the overriding plate. Above the Peruvian flat-slab, a 200 km-long normal fault trend parallel to the range and delimits the western flank of the Cordillera Blanca. In a context of flat subduction, expected to produce shortening, the presence of the Cordillera Blanca normal fault (CBNF) is surprising. We performed a systematic inversion of striated fault planes in the Cordillera Blanca region to better characterize the stress field above the Peruvian flat-slab. It evidences the succession of different tectonic regimes. NE-SW extension is predominant in most of the sites indicating a regional extension. We suggest that the Peruvian flat-slab trigger extension in the Western Cordillera while the shortening migrated eastward. Finally, we propose that flat-slab segments do not increase the coupling at the trench neither the shortening in the overriding plate but only favor shortening migration backward. However, the stress field of the overriding plate arises from the evolution of plate interface properties through time due to bathymetric anomaly migration.

© 2017 Elsevier Ltd. All rights reserved.

## 1. Introduction

The western South American margin is segmented along-strike, with changing Andean topography and slab dip variations (Barazangi and Isacks, 1976). Two flat-slab segments have been identified by seismological data in northern Peru (3—15°S) and central Chile (28—32°S) (Barazangi and Isacks, 1976, Fig. 1). In such subduction settings, the tectonic regime of the overriding plate is closely related to the convergence direction, dip and geometry of the subducting plate (Ramos and Folguera, 2009). Around the world, flat-slab segments appear to increase coupling at the plate interface, resulting in both an increase and eastward migration of the shortening in the overriding plate (Jordan et al., 1983; Ramos and Folguera, 2009; Martinod et al., 2010).

Above the Peruvian flat-slab, a striking 200 km-long normal fault trending parallel to the range delimits the western flank of the Cordillera Blanca high peaks (Bonnot, 1984; McNulty and Farber, 2002; Giovanni, 2007). Those peaks (>6000 m) are abnormally

higher than the average plateau altitude at this place (~4400 m). In such a context of flat subduction, expected to produce shortening, the joint presence of the Cordillera Blanca normal fault (CBNF) with high reliefs is surprising. Indeed, despite regional expected shortening related to the flat-slab subduction of the Nazca Plate beneath the South America, the Cordillera Blanca normal fault has been active during the Quaternary. Two models have been proposed to explain the occurrence of extension in this part of the high Andes: Dalmayrac and Molnar (1981) suggested an extensional collapse of a thickened crust, whereas McNulty and Farber (2002) involved oceanic ridge buoyancy under the Cordillera Blanca. Despite these models, the tectonic setting of the Cordillera Blanca emplacement is still debated: while Petford and Atherton (1992) suggested that the Cordillera Blanca batholith has emplaced in a dextral wrench regime based on ductile deformation structures, McNulty et al. (1998) interpreted some magnetic susceptibility data from the batholith as the result of a sinistral wrench regime.

As this opposition extension versus along strike shearing is a key issue for Andean geodynamics (e.g., Dewey and Lamb, 1992; McNulty et al., 1998; Taylor et al., 1998; Scheuber and Gonzalez, 1999; Folguera et al., 2006, Audin et al., 2008), the aim of this paper is to precise and constrain the stress field evolution through

* Corresponding author. Now at Helmholtz Zentrum Potsdam, Geo-ForschungsZentrum (GFZ) Potsdam, Potsdam, Germany.
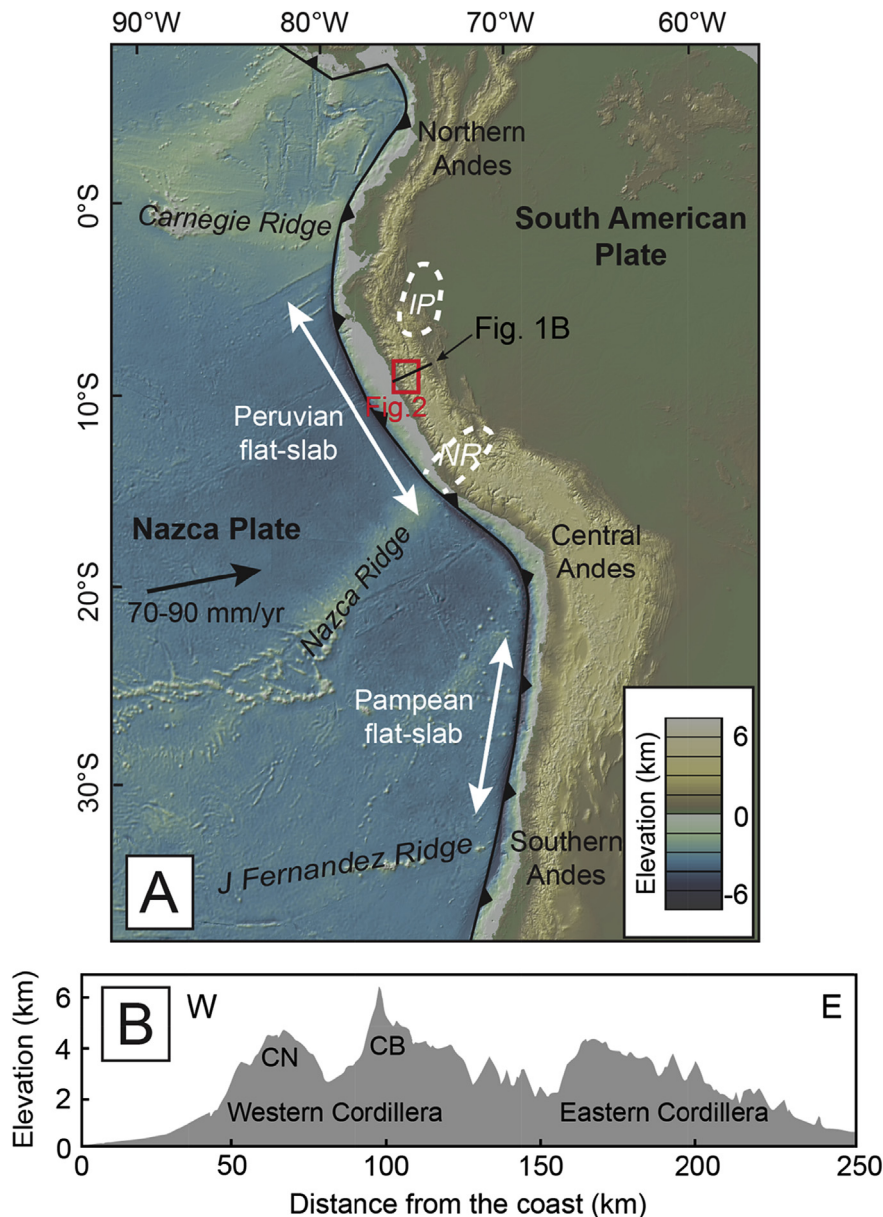*E-mail address:* audrey.margirier@gmail.com (A. Margirier).

**Fig. 1.** A) Topographic map of the Andes (SRTM data) including flat slab segments and bathymetric features as the Nazca Ridge (NR) and the Inca plateau (IP; Inca Plateau location after Gutscher et al. (1999)). The study area is indicated by the red rectangle. B) Topographic cross-section of the Peruvian Andes at the latitude of the Cordillera Blanca showing the Cordillera Blanca (CB), the Cordillera Negra (CN), the Western Cordillera and the Eastern Cordillera. (For interpretation of the references to colour in this figure legend, the reader is referred to the web version of this article.)

time in this region with new microstructural data. Indeed, analyzing the ductile and brittle tectonic deformation in the crust permits to describe the impact of flat subduction on the stress field in the overriding plate in northern Peru. Moreover, the knowledge of the regional stress field evolution could provide information on processes driving the Cordillera Blanca batholith exhumation. The stress field evolution above the flat-slab is mainly inferred from inversions of striated fault planes measured on different outcrops in the Cordillera Blanca region.

## 2. Geodynamic and tectonic context of northern Peru

### 2.1. Geodynamic setting

The Andes are the result of the long-lasting subduction of the Nazca Plate beneath the South America Plate. The subduction zone has been active since at least Cretaceous time, with convergence rates, obliquity and subduction dip changing through time (e.g., Somoza, 1998; Ramos and Folguera, 2009; Martinod et al., 2010). These changes have been associated to different tectonic phases affecting the Andean range (e.g., Jordan et al., 1983; Pardo-Casas and Molnar, 1987; Somoza, 1998) and influenced the magmatic activity along strike (Kay and Kay, 2002; Ramos and Folguera, 2009).

The northern Peruvian margin displays a present-day flat sub-duction zone where both, the geometry and timing of slab flat-tening are well constrained for the last 15 Ma (e.g., Gutscher et al., 1999; Hampel, 2002; Rosenbaum et al., 2005; Antonijevic et al., 2015). Gutscher et al. (2000) suggested that the flat-slab has a ~20 km deep sag between the Nazca Ridge and the Inca Plateau

thickened parts (Fig. 1). The subduction of these two buoyant features have been proposed to induce the slab flattening in northern Peru (Gutscher et al., 1999). Based on this hypothesis, several reconstructions of the timing and location of the initial Nazca Ridge subduction based on symmetric seafloor-spreading in a hotspot reference frame constrained the timing of the slab flattening (e.g., Hampel, 2002; McNulty and Farber, 2002; Rosenbaum et al., 2005; Antonijevic et al., 2015). However, all of these models rely on calculations of the motion of the Nazca Plate with respect to South America, which may induce considerable errors. Rosenbaum et al. (2005) presented a regionally refined plate circuit that suggests the initiation of the Nazca Ridge subduction at 15 Ma at 10°S and the arrival of the Inca Plateau at 13 Ma at 5°S. This reconstruction, in agreement with the timing of magmatism migration eastward, indicates that the slab flattening occur at the latitude of the Cordillera Blanca region from ~15 Ma.

## 2.2. Peruvian tectonic history

Several tectonic phases corresponding to short tectonic events that seems to have largely contributed to the Andean range building have been identified (Mégard, 1984). The first known major compressional event occurred in Late Albian, (113.0–100.5 Ma; Mégard, 1984). This tectonic phase, named Mochica, is recorded in the whole Western flank of the Central Andes (Jaillard, 1994) and is characterized by NE-SW compression (Mégard, 1984) likely associated with a dextral wrenching component (Bussel and Pitcher, 1985). It has been followed by a widespread episode of deformation in Peru, named the Peruvian phase, during the Santonian and the Campanian (86.3–70.6 Ma, NE-SW compression; Steinmann, 1929; Mégard, 1978; Gayet et al., 1991, Jaillard, 1993; Jaillard and Soler, 1996). An episode of uplift is likely contemporaneous with Peruvian phase in the Western Cordillera (Mégard, 1984). Then, from mid to late Eocene the main Andean shortening phase, the Incaic phase, caused extensive folding and reverse faulting in the Jurassic sediments of the Western Cordillera and the formation of a fold and trust belt along the Western Cordillera in Central Andes (48.6–33.9 Ma, NE-SW compression; Mégard, 1984; Noble et al., 1990).

The Neogene tectonic phase named the Quechua phase is divided in three discrete phases (e.g., McKee and Noble, 1982; Mégard, 1984; see Fig. 9). The Quechua 1 phase (20–12.5 Ma) is characterized by NW-SE shortening and by reactivation of structures inherited from the Incaic phase in northern Peru, from the Western Cordillera to farther east. It seems that the deformation associated with the Quechua 1 phase reached the Eastern Cordillera (Mégard, 1984). The Quechua 2 is bracketed between 9.5 and 8.2 Ma in central Peru (Mégard et al., 1984). This phase is characterized by dextral strike-slip along NW-SE structures likely caused by N-S compression (Soulas, 1977). Finally, the Quechua 3 phase identified in the subandean fold and thrust belt (~6 Ma; Mégard, 1984) is characterized by E-W compression (Soulas, 1977).

## 2.3. Geologic and Quaternary tectonic settings of the Cordillera Blanca region

The Cordillera Blanca and the Cordillera Negra are located in the northern Peruvian Andes, in the Western Cordillera (Fig. 1). The Cordillera Blanca is a Miocene granitic pluton (14-5 Ma; Mukasa, 1984; McNulty et al., 1998; Giovanni, 2007) emplaced in deformed Jurassic sediments of the Chicama Formation at pressures ranging from 100 to 200 MPa (Petford and Atherton, 1992; Margirier et al., 2016). The Cordillera Blanca batholith and associated magmas, the Fortaleza and Yungay ignimbrites emplaced respectively around 7.4 Ma (Wipf, 2006) and between 8 and 3 Ma

(Wise and Noble, 2003; Giovanni, 2007; Giovanni et al., 2010), correspond to the last magmatic activity before the cessation of magmatism associated to the slab flattening in northern Peru (Petford and Atherton, 1992).

The high summits of the Cordillera Blanca correspond to the footwall of the CBNF. The elongated shape (trending parallel to the Andean range) and the internal fabric of the batholith suggest its emplacement along a pre-existing lithospheric fault structure, in a strike-slip context (Cobbing et al., 1981; Petford and Atherton, 1992; McNulty et al., 1998). However, there is no consensus about the kinematics: dextral (based on ductile sub-solidus fabric in the granite and on en-echelon structure in pegmatites; Petford and Atherton, 1992) versus sinistral (from unclear AMS fabric; McNulty et al., 1998).

Preliminary studies addressed the Cordillera Blanca brittle tectonic history with microtectonic data and stress reconstructions from fault slip dataset inversion (Bonnot, 1984; Sébrier et al., 1988). Bonnot (1984) proposed the succession of the following tectonic phases: (I) Pliocene E-W extension ($\sigma_3$ sub-horizontal N285, $\sigma_1$ sub-vertical), (II) Quaternary E-W compression ($\sigma_1$ sub-horizontal N080, $\sigma_3$ sub-vertical) and N-S compression ($\sigma_1$ sub-horizontal N150, $\sigma_3$ sub-vertical), (III) N-S extension from the Pleistocene to present day ($\sigma_3$ sub-horizontal N0, $\sigma_1$ sub-vertical). Sébrier et al. (1988) only focused on the last fault slip and suggested N-S extension in the Cordillera Blanca. Neither the Quaternary compression nor the N-S extension they evidenced in the Cordillera Blanca is in agreement with present day extensional microseismicity (Deverchère et al., 1989).

The general trend of the Cordillera Blanca fault zone is N140° dipping 35–45°SW. Variations of the scarp heights and en echelon faulting in the southern part of the fault show that the CBNF is segmented (Fig. 2; Giovanni, 2007). Field studies evidence discontinuous NW-SE striking scarps that displace Quaternary glacial moraines as well as plutonic rocks (Fig. 3; e.g., Bonnot, 1984; Schwartz, 1988). Along the fault zone, repeated displacements imprinted the landscape, with ~2 to >100 m-high scarps, corresponding to vertical displacements cumulated during the Quaternary (Fig. 3B and C) and ~1 km-high triangular facets (Fig. 3A). In total, considering the emplacement depth of the Cordillera Blanca batholith, the scarps height and the basin sedimentary filling thickness, the CBNF shows at least 4500 m of vertical displacement in its central part since ~5 Ma (Bonnot, 1984; Giovanni, 2007; Margirier et al., 2016).

Based on thermochronologic data (apatite fission-tracks and apatite (U-Th)/He), Giovanni (2007) and Hodson (2012) gave estimation of exhumation rate at ~2 mm/yr and >1 mm/yr respectively on the central part of the CBNF and decreasing exhumation rates toward the South for the last 3 Ma. For the last 4 Ma, Margirier et al. (2015), based on the same thermochronologic systems, suggest lower exhumation rate (1 mm/yr) for the central part of the Cordillera Blanca. Even if modeling of thermochronologic ages did not indicate a well-defined north-south trend in erosion rate (Margirier et al., 2016) the total exhumation since the batholith emplacement decreases in the southern part of the Cordillera Blanca (Margirier et al., 2016). Based on the CBNF morphology and the Cordillera Blanca geology Bonnot (1984) estimated vertical slip rates of ~0.7 mm/yr on the CBNF between 3 and 0 Ma. On a more recent time scale (30-0 ka), the CBNF displacement rates have been constrained by [10]Be dating of scarps (Siame et al., 2006) and geomorphic features (moraines) displaced by the fault (Fig. 3B and C; Schwartz, 1988; Farber and Hancock, in prep). The vertical slip rates decrease from north to south ranging from 5.1 ± 0.8 mm/yr to 0.6 ± 0.2 mm/yr (Fig. 2B; Schwartz, 1988; Siame et al., 2006; Farber and Hancock, in prep).

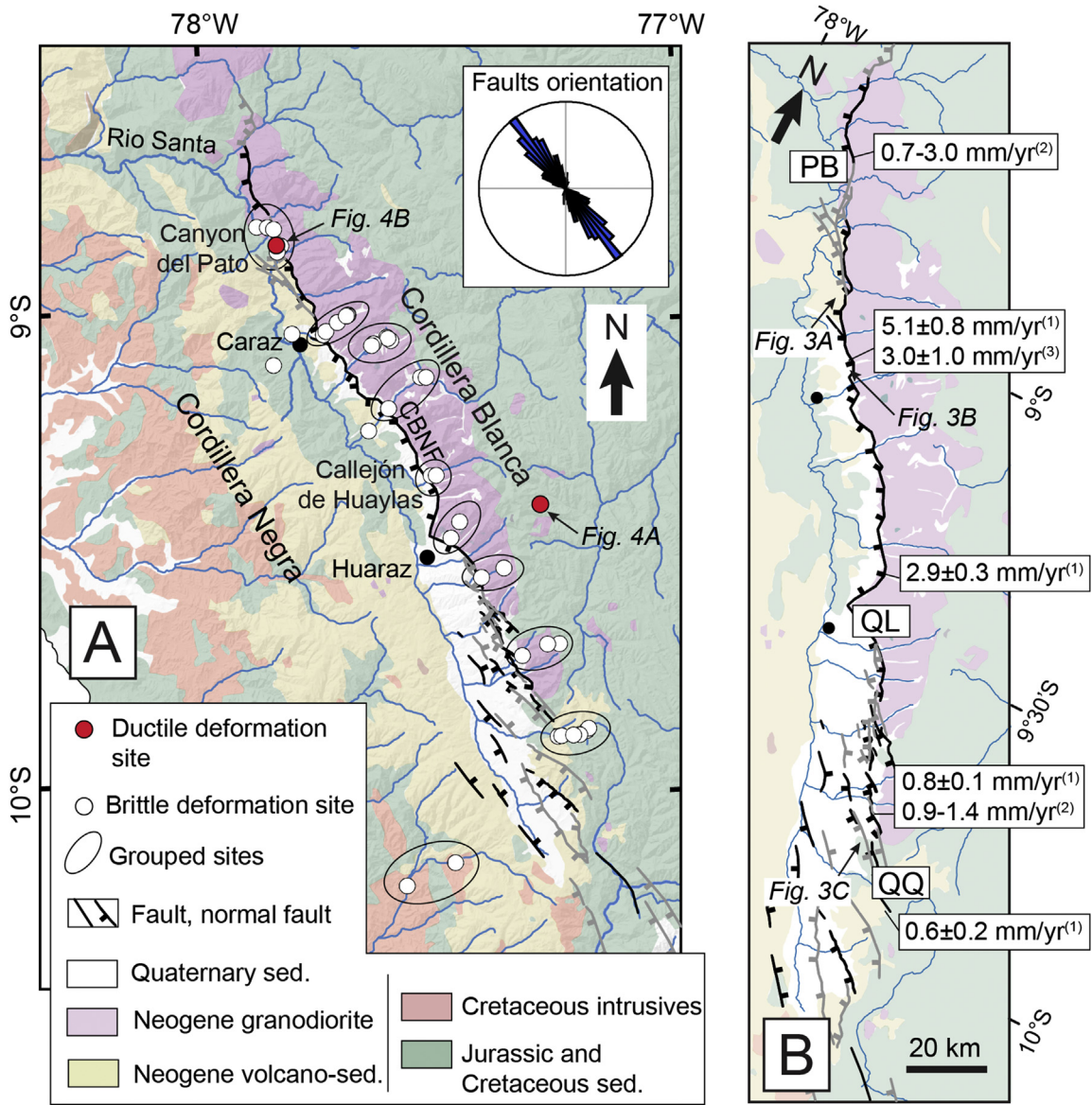In terms of seismic activity, no historical earthquake has been

**Fig. 2.** Geological maps of the study area. A) Map showing the active faults mapped in this study (black lines) and from Neotectonic Open Database (grey lines), the measurement stations (white dot), the grouped sites and the sites where ductile deformation was analyzed (red dot). Inset shows a rose diagram of the fault segments azimuth B) Zoom on the CBNF with Quaternary vertical slip-rates from [1]Farber and Hancock (in prep), [2]Schwartz (1988) and [3]Siame et al. (2006) and location of bedrock slickensides measurement sites along the CBNF (Pachma Bajo, PB; Quebrada Llaca, QL and Quebrada Querococha, QQ). (For interpretation of the references to colour in this figure legend, the reader is referred to the web version of this article.)
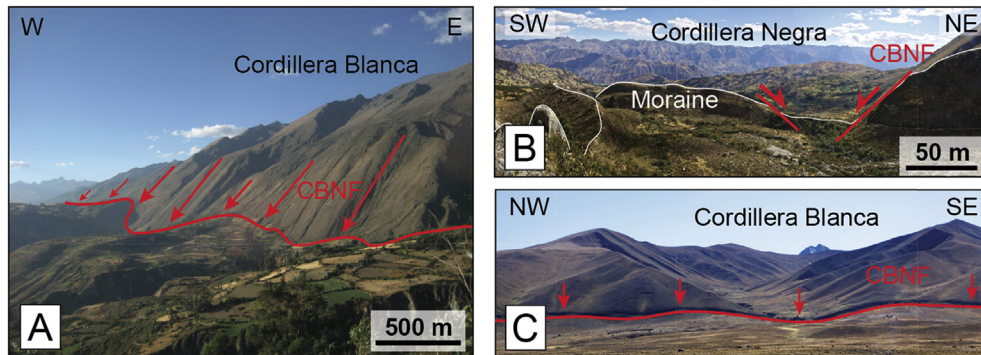


**Fig. 3.** Photographs of the CBNF. See Fig. 2B for locations. A) Triangular facets in the northern part of the Cordillera Blanca (1000 m high). B) Moraine offset at the outlet of the Quebrada Huaytapallana (offset ~100 m). C) Quaternary scarp in the Lloclla Formation (southern Cordillera Blanca) (offset ~4 m).
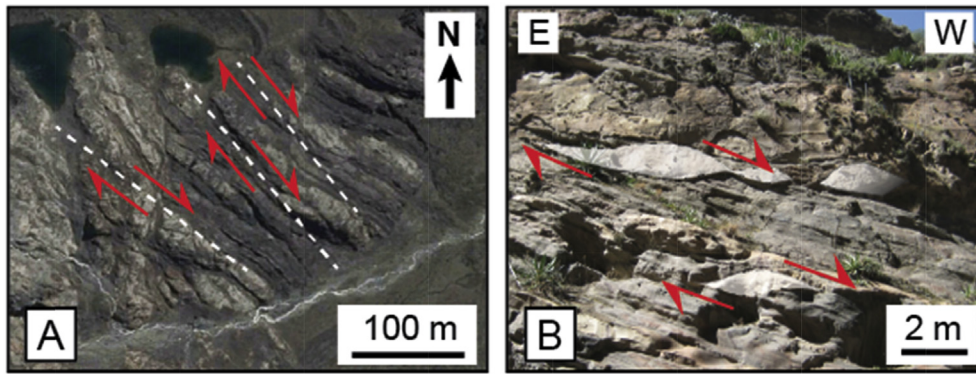
**Fig. 4.** Ductile deformation in the Cordillera Blanca (see Fig. 2 for location). A) Google Earth Landsat image with dextral strike-slip in the eastern Cordillera Blanca, about 20 km East from the CBNF. B) Photograph of the ductile deformation of dykes in the cliffs of the Canyon del Pato, in the CBNF zone.

reported for the CBNF (Silgado, 1992). However, some microseismicity occurs in the Cordillera Blanca region. The focal mechanisms indicated present-day NE-SW extension in adequacy with Quaternary offsets along the CBNF (Deverchère et al., 1989). The most significant coseismic surface faulting has been reported in 1946 along the Quiches normal fault (Mw = 6.8; Doser, 1987; Bellier et al., 1991), 50 km north-east from the CBNF trace. No significant seismic event (Mw > 4) has been reported South of the CBNF segments neither along the Cordillera Huayhuash neither farther South (Neotectonic Open Database[1]).

West of the Cordillera Blanca, the Callejón de Huaylas, an elongated range-parallel intra-mountain basin (150 km long), builds the hanging wall of the CBNF and separates the Cordillera Blanca and the Cordillera Negra. The sedimentary series filling this intra-mountain basin recorded its subsidence associated to the CBNF initiation and activity (Bonnot, 1984). Indeed, at the base of the series some ignimbrites dated at 5.4 ± 0.1 Ma suggest that normal faulting initiated at least at ~5.4 Ma (Giovanni, 2007; Giovanni et al., 2010). Westward, the Cordillera Negra consists of Cretaceous and Paleogene plutons (73-48 Ma; Mukasa, 1984; Beckinsale et al., 1985) intruded in the Chicama formation. Neogene volcano-sedimentary deposits capped the older formations in the southern part of the Cordillera Negra.

## 3. Methods

### 3.1. Satellite image analysis

In mountain ranges, the landscapes are largely controlled by the lithology and tectonic structures. Fracturing favors chemical weathering and weaken the rocks. Satellite imageries can be used to map fractures at up to kilometers scale in rocky landscapes/areas. Here, we analyzed satellite images (Google Earth, Landsat images, 2001–2002, visible band with a space resolution of 15 m) to map the main faults at regional/km scale (Fig. 2). Mapping displacements along active faults is based on displacement of surfaces or geomorphic markers such as moraines or Quaternary pediment surfaces. For each lineament we checked if it corresponds to a fault and not to a fold axis or a stratigraphy boundary (Fig. 2). To discuss the contradictory conclusions of previous works on the ductile deformation in the Cordillera Blanca (Petford and Atherton, 1992; McNulty et al., 1998), we also collected ductile deformation data in the field and from satellite image (Google Earth, Landsat images; Fig. 4).

---

[1] neotec-opendata.com.

### 3.2. Tectonic stress inversion

#### 3.2.1. Principe

Several methods, based on sets of fault planes and slickenlines, permit to estimate paleostress tensors (e.g., Angelier and Mechler, 1977; Angelier, 1984). The reduced stress tensor, obtained from faults-slickenlines pairs inversion, provides the orientation of the principal stress axes $\sigma_1$, $\sigma_2$, $\sigma_3$ (with $\sigma_1 > \sigma_2 > \sigma_3$ and compression being positive) and a shape parameter that we defined here as $Phi = (\sigma_2 - \sigma_3)/(\sigma_1 - \sigma_3)$ (e.g., Angelier, 1984; Delvaux and Sperner, 2003). These inversion methods rely on three assumptions: (a) the stress is uniform in the volume of rock considered, (b) the stress tensor is equivalent to the incremental deformation tensor as obtained from the slip data, and (c) the slip vector on a fault plane (given by the slickenlines) is parallel to the maximum shear stress along the plane as deduced from the stress tensor (Bott, 1959). These assumptions imply careful choice of the measurement stations, and brittle deformation measurements.

#### 3.2.2. Fieldwork

We measured more than 400 couples fault-slickenline on 38 sites in the Cordillera Blanca region (Table 1). For each site we measured between 2 and 34 striated fault planes (supplementary tables A1 and A2, for all the planes we measured dip direction and dip angle) on outcrops no larger than 50 m with homogenous lithology. We measured all the striated planes we have been able to see on the outcrops without selection. We constrained the displacement direction and sense on each fault plane with classical tectoglyphs (fibers, striations, steps …). For each measurement we attributed a qualitative confidence level for the sense of the displacement found on the field (supplementary table A2). We kept only the striated planes with unambiguous displacement sense. For "natural" outcrops, fault planes are weathered and the slickenlines are not well preserved, leading to too few measurements to be able to use them for analysis. Most of our sites are located along roads for quality of outcroppings: it is constituted of fresh rocks and most of the faults-planes and slickenside striae sets can be measured (orientation and dip). Measurement sites are mostly located in the Cordillera Blanca but few stations are in the Cordillera Negra and the Callejón de Huaylas (Fig. 2). This heterogeneous sampling is related to difficulties to find sites with competent, fractured and low weathered rocks in the Cordillera Negra.

#### 3.2.3. Inversion methods

Different computer softwares are available to determine the reduced stress tensor that best explains the slip distribution on a set of fault planes (e.g., TectonicsFP, FaultKinWin, TENSOR,

**Table 1**
Stress tensors from grouped sites.

| Site | Tensor | Number of couples fault/striation | PBT | | | | Right diedra | | | |
| --- | --- | --- | --- | --- | --- | --- | --- | --- | --- | --- |
| | | | Phi | Sigma 1 | Sigma 3 | Maximum angular deviation (°) | Phi | Sigma 1 | Sigma 3 | Maximum angular deviation (°) |
| **Canyon del Pato** | **128** | | | | | | | | | |
| | T1 | 66 | 0.53 | 85/146 | 01/234 | 30 | 0.51 | 77/149 | 00/058 | 30 |
| | T2 | 12 | 0.44 | 04/095 | 15/005 | 28 | 0.42 | 15/090 | 11/357 | 32 |
| | T3 | 11 | 0.50 | 38/171 | 14/068 | 29 | 0.64 | 42/181 | 25/066 | 25 |
| **Caraz** | **34** | | | | | | | | | |
| | T1 | 9 | 0.53 | 53/108 | 31/251 | 33 | 0.67 | 54/106 | 33/259 | 24 |
| | T2 | 10 | 0.58 | 66/295 | 20/086 | 34 | 0.55 | 62/328 | 19/099 | 34 |
| | T3 | 8 | 0.70 | 07/265 | 74/165 | 42 | 0.69 | 00/264 | 67/174 | 30 |
| **Pueblo Libre** | **12** | | | | | | | | | |
| | T1 | 12 | – | – | – | – | 0.62 | 61/197 | 02/103 | 30 |
| **Laguna Paron** | **60** | | | | | | | | | |
| | T1 | 15 | 0.48 | 72/117 | 12/245 | 33 | 0.32 | 65/124 | 17/255 | 27 |
| | T2 | 16 | 0.45 | 12/201 | 31/103 | 34 | 0.44 | 10/194 | 31/098 | 30 |
| | T3 | 6 | 0.51 | 56/085 | 14/197 | 26 | 0.67 | 60/081 | 17/202 | 26 |
| **Quebrada Llanganuco** | **58** | | | | | | | | | |
| | T1 | 23 | 0.50 | 65/045 | 25/235 | 34 | 0.56 | 59/104 | 17/226 | 43 |
| | T2 | 8 | 0.50 | 52/010 | 06/109 | 32 | 0.56 | 58/006 | 07/108 | 32 |
| **Quebrada Ulta** | **63** | | | | | | | | | |
| | T1 | 27 | 0.50 | 70/275 | 17/061 | 33 | 0.56 | 66/282 | 17/053 | 35 |
| | T2 | 13 | 0.49 | 12/252 | 62/011 | 30 | 0.46 | 07/258 | 79/027 | 32 |
| | T3 | 6 | 0.50 | 52/112 | 10/011 | 29 | 0.50 | 61/103 | 10/355 | 37 |
| **Quebrada Honda** | **15** | | | | | | | | | |
| | T1 | 9 | 0.44 | 50/026 | 32/240 | 31 | 0.25 | 43/033 | 39/254 | 26 |
| **Quebrada Llaca** | **14** | | | | | | | | | |
| | T1 | 6 | 0.50 | 32/256 | 50/036 | 27 | 0.67 | 01/123 | 56/031 | 44 |
| **Quebrada Rajucolta** | **21** | | | | | | | | | |
| | T1 | 7 | 0.50 | 76/233 | 14/057 | 24 | 0.57 | 69/225 | 21/058 | 35 |
| | T2 | 7 | 0.56 | 16/305 | 04/212 | 24 | 0.57 | 13/303 | 09/211 | 19 |
| **Quebrada Queroccocha** | **70** | | | | | | | | | |
| | T1 | 15 | 0.50 | 59/025 | 24/163 | 30 | 0.47 | 68/032 | 18/251 | 39 |
| | T2 | 16 | 0.44 | 59/130 | 19/005 | 32 | 0.34 | 67/146 | 16/013 | 32 |
| | T3 | 8 | 0.61 | 05/346 | 27/080 | 30 | 0.62 | 12/346 | 28/083 | 25 |
| | T4 | 6 | 0.54 | 07/041 | 10/133 | 33 | 0.67 | 04/229 | 22/137 | 31 |
| **Quebrada Pastoruri** | **89** | | | | | | | | | |
| | T1 | 25 | 0.57 | 57/171 | 11/061 | 34 | 0.60 | 52/162 | 12/056 | 31 |
| | T2 | 16 | 0.46 | 50/264 | 18/015 | 33 | 0.50 | 35/258 | 29/011 | 33 |
| | T3 | 6 | 0.63 | 46/125 | 29/232 | 28 | 0.75 | 50/123 | 30/257 | 21 |
| **Fortaleza Valley** | **14** | | | | | | | | | |
| | T1 | 7 | 0.55 | 17/326 | 00/230 | 35 | 0.50 | 31/312 | 06/046 | 38 |

WinTensor, Mim; Marrett and Allmendinger, 1990; Sperner et al., 1993; Yamaji, 2000; Ortner et al., 2002; Delvaux and Sperner, 2003; Delvaux, 2012). As they are based on the same physical concepts, all these methods are expected to give similar results (Delvaux and Barth, 2010; Lacombe, 2012). The inversion of the data was here performed using the software WinTensor (Delvaux, 2012) which inverts a dataset with the right dihedra method (Angelier and Mechler, 1977) and the PBT method (Angelier, 1984). In the right dihedra method an auxiliary plane is defined, orthogonal to the striated plane and to the striae. The striated plane and the auxiliary plane define 4 right dihedras and 2 half spaces: a shortening half-space and an extensional half-space, defined by the kinematic of the striaes. All results are then superimposed and a statistical outline is used to calculate a tensor with $\sigma_1$ in dihedra in compression and $\sigma_3$ in dihedra in extension. This initial result is used by the "Rotational Optimisation" procedure that minimizes, by an iterative grid search, the misfit angle (Delvaux and Sperner, 2003). Based on Wallace (1951) and Bott (1959) principles, the PBT method considers that the slip vector on a fault plane is parallel to the maximum shear stress along the plane. For each striated plane, compression and extension axis (P and T-axis) are constructed, both lying in the plane given by the shear plane normal and the slickenline. In homogeneous materials, $\sigma_2$ lies in the fault plane, and $\sigma_1$ and $\sigma_3$ in the plane containing the fault-plane normal and the striae.

The inversion requires at least 5 fault-slickenline pairs. A higher number of data better constrains the solution. Here, we used at least 6 pairs of fault-slickenline for an inversion. The angular misfit between the measured slickenline and the theoretical slickenline predicted from the calculated tensor is used as a quality indicator of the inversion (Fig. 5).

We processed the data following a multistep approach (Zeilinger et al., 2000). A random tensor search was performed for each site (or grouped sites). The data is rejected when the misfit between the slickenline and the theoretical slickenline predicted from the calculated tensor is > 30°. Then, all the rejected striated planes are recovered and the same procedure was applied. Populations of less than 6 striated planes were considered not significant. For each valley when our sites are close to each other (stations distributed in an area smaller than 10 km), we group the sites located in tectonically homogeneous units to process them as single sites and average the regional stress field (Zeilinger et al., 2000; Pêcher et al., 2008). The larger number of fault-slickenline pairs for grouped sites permits a more robust determination of tensors.
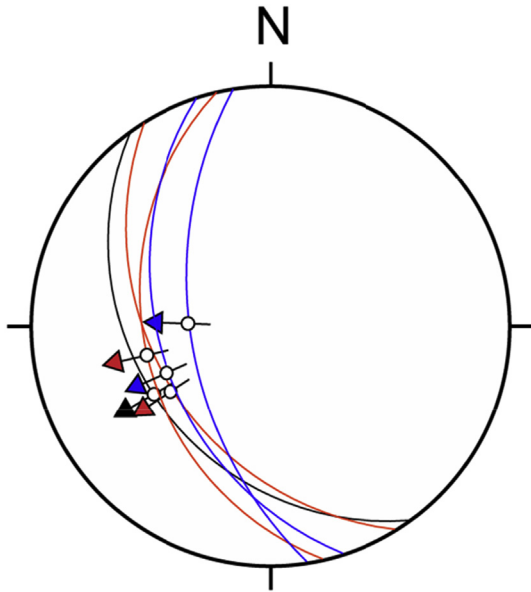
**Fig. 5.** Cordillera Blanca fault planes and striaes orientation and dip, Wulff lower hemisphere stereographic projection. Measurements were done in Pachma Bajo (PB; blue), Quebrada Llaca (QL; black) and Quebrada Querococha (QQ; red), see Fig. 2B for the location of the sites. (For interpretation of the references to colour in this figure legend, the reader is referred to the web version of this article.)

## 4. Results

### 4.1. Ductile deformation and local cooling ages of the Cordillera Blanca batholith

We analyzed punctual ductile deformation evidences during the fieldwork and from satellite images to discuss the tectonic context during the Cordillera Blanca batholith emplacement. The granitic veins developed in the sediments close to the batholith contact are good deformation markers ranging from field to satellite scale. Their ductile deformation provides a reliable constraint of the upper plate regional strain axes contemporary of their emplacement.

Along the eastern limit of the Cordillera Blanca batholith, some deformed dykes intruded the Jurassic sediments and indicates a dextral sense of shearing along the batholith (Figs. 2 and 4A). The surrounding granite is dated at ~8 Ma (zircon U-Pb and muscovite Ar-Ar; Giovanni, 2007).

In the Cordillera Blanca batholith a penetrative foliation and S-C structures indicates normal top to SW sense of shearing. In addition, in the Canyon del Pato close to the contact between the batholith and sediments, a dyke complex intrudes sedimentary rocks of the Chicama Formation. Its ductile deformation indicates normal top to SW sense of shearing and NE-SW extension (shearing plane = N145 30SW, stretching lineation = N50 20SW; Fig. 4B). Close to this outcrop, the Cordillera Blanca batholith cooling is younger, ages range from 5 to 3.6 Ma (muscovite Ar-Ar and K-Ar; Stewart et al., 1974; Giovanni, 2007).

### 4.2. Brittle deformation

#### 4.2.1. The Cordillera Blanca normal fault

Along strike the fault displays a well-defined scarp developed either in the bedrock, in Quaternary alluvial fan, moraines or debris-flow deposits attesting of repeated displacements. Field surveys evidence cumulative scarp height decreasing in lower and younger deposits, it suggests multiple Holocene faulting events preserved on each sites. Southwards, the Holocene fault scarp

varies from a well-defined single scarp tens m-high to several sub-parallel en echelon faulting of about 1 m-high. Punctually, the fault trace splits down in the Callejon de Huaylas into small graben and antithetic scarps, adjacent to the main scarp (Fig. 2). Northwards, the Quaternary scarp (strike N140°) displays an impressive and constant westward dip of ~35–45°.

Along the CBNF several sites display striaes on the fault plane: from North to South, in Pachma Bajo, Quebrada Llaca and Quebrada Querococha (Fig. 2B). Striae on the fault have a down dip direction (N249-39SW). Tectoglyphs indicate a normal sense displacement (Fig. 5) consistent with the Quaternary displacement of the moraines along the CBNF (Dalmayrac and Molnar, 1981; Bonnot, 1984). This normal fault accommodates an ENE-WSW extension. Bonnot (1984) also reports bedrock slickensides along the fault scarp between Chiquian and Huaraz. He suggested that there might have been a sinistral component to the Quaternary slip on the fault segments striking N110 to N155. The en-echelon faults striking N140 in the southern part of the CBNF also suggest a sinistral component (Bonnot, 1984). However, the cumulated amount of such strike-slip component must be negligible because lateral offsets of moraine axes are not observed on the field.

#### 4.2.2. Example of a multistep deformation history in the Canyon del Pato

In the Canyon del Pato, we collected data from 5 sites spread along a 5 km-distance. All the sites are located in the Cordillera Blanca batholith close to the CBNF (Fig. 2). We measured in this area 128 fault-slickenline pairs in the Neogene bedrock (Fig. 6). Here, a single stress tensor cannot explain our data; the angular deviation is > 50° for ~50% of the data. The important dispersion of fault orientations (Fig. 6) suggests a multistep brittle deformation history. Following this hypothesis, we obtained 3 stress tensors from faults-slickenlines inversion. Labeling T1, T2 and T3 refer only to the number of striated planes associated to each tensor and didn't imply a chronology. The predominant tensor (T1, 66 faults) corresponds to NE-SW pure extension (Fig. 6). The second stress tensor (T2, 12 faults) is related to E-W transpression with a component in sinistral strike-slip. The less well-defined third stress tensor (T3, 11 faults) corresponds to E-W pure extension. None of the T3 axes is vertical indicating that this tensor has been tilted while T1 and T2 seem not tilted. It could indicate that T3 is the older tensor.

#### 4.2.3. Regional stress fields

Most of our measurements were taken in the Cordillera Blanca batholith. In addition, five sites are located in the southern part of the Cordillera Blanca (Quebrada Pastoruri), in sedimentary and volcanic rocks, one is in the Callejón de Huaylas (Caraz) and two sites are located in the Cordillera Negra (Fortaleza Valley and Pueblo Libre). The results of stress tensors for grouped sites are presented in the Table 1. For the best-defined tensor (T1) most of the misfit are lower than 15° demonstrating the quality of the inversion, for the other tensors (T2 and T3) most of the misfit are lower than 20°.

The Cordillera Blanca brittle deformation reflects the recent stress field that is superimposed on ductile deformation acquired during the Cordillera Blanca emplacement and early exhumation. In most of the sites we found up to two tensors with different characteristics (extension, wrenching and compression). The wide range of tensors suggests a multistep brittle deformation history in the Cordillera Blanca region. The best-expressed stress tensor corresponds to NE-SW extension (80% of the 38 sites; Figs. 7 and 8A). The extension is not restricted to the Cordillera Blanca. Indeed, the Pueblo Libre and the Fortaleza sites recorded respectively E-W extension and transtension with horizontal E-W σ₃ axis. The stress inversion also indicates wrenching (50% of the sites), N-S extension
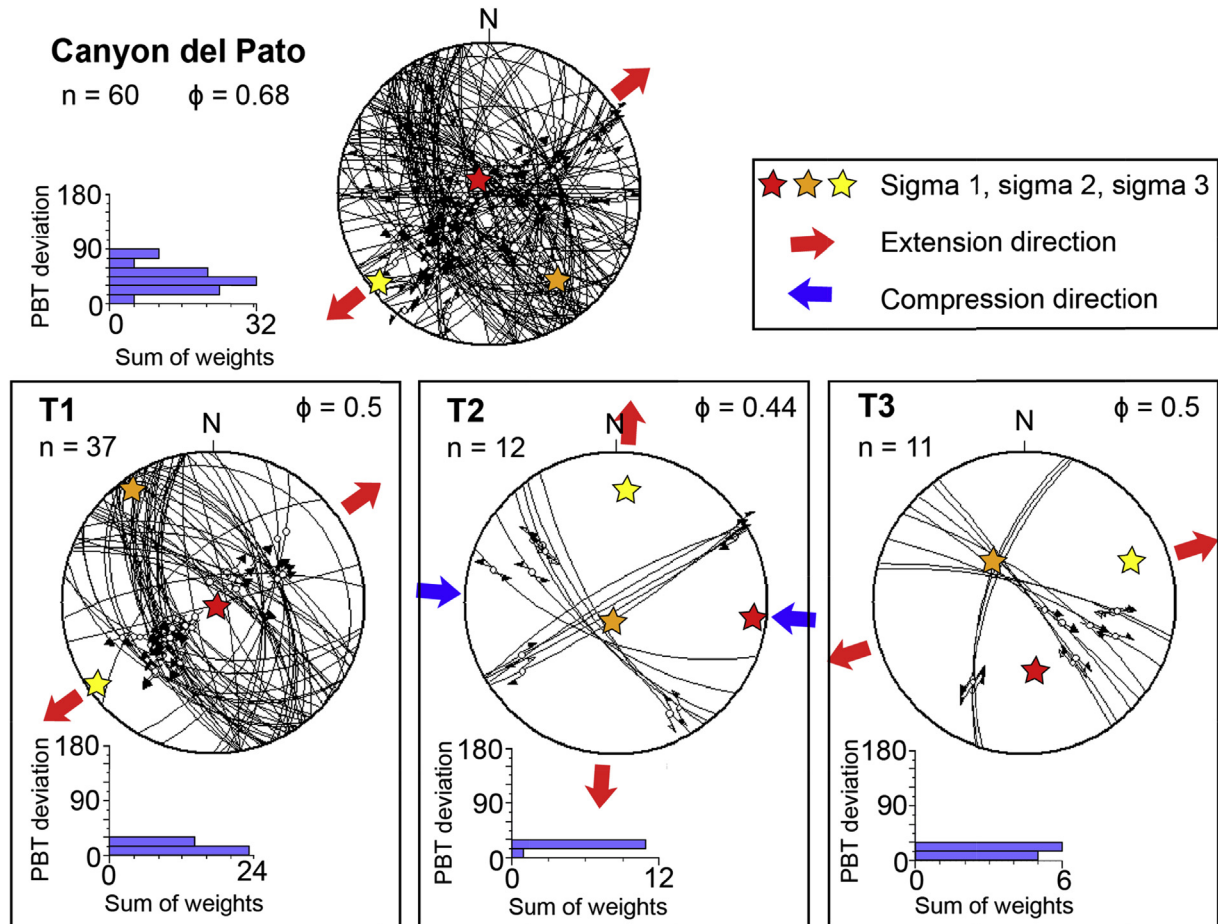
**Fig. 6.** Faults in the Canyon del Pato (Cordillera Blanca), Wulff lower hemisphere stereographic projection. A) All faults measurements and associated tensor calculation (PBT method) the angular deviation is shown by the histogram, *n* corresponds to the number of fault measurements for each tensor, *Phi* corresponds to a shape parameter defined here as $Phi = (\sigma_2 - \sigma_3)/(\sigma_1 - \sigma_3)$. B-D) Tensors T1, T2, T3 and related fault-slickenline pairs (see text for tensor determination method).

(in Quebradas Ulta, Querococha and Pastoruri, 30% of the sites) and E-W compression (in Quebradas Llaca and Ulta, 15% of the sites) (Figs. 7 and 8). The E-W compression tensors indicate that a compressional phase affect the Cordillera Blanca region after the Cordillera Blanca emplacement. Therefore, after ~8 Ma several tectonic regimes followed one another in the Cordillera Blanca region (see Fig. 9).

## 5. Discussion

### 5.1. Tectonic context for the Cordillera Blanca emplacement

Our ductile deformation data indicates two different strain regimes: a dextral strike-slip in the eastern part of the Cordillera Blanca (Fig. 4A, see Fig. 2 for site location) and an E-W extension close to the CBNF, in the northern part of the Cordillera Blanca (Fig. 4B). As the Cordillera Blanca batholith displays different ages in these two sites and as the deformation indicates two different strain regimes, these two regimes may result from different tectonic phases (Fig. 9).

First, the granite emplaced in a dextral strike-slip regime (~8 Ma, Fig. 4A). Our data are here in agreement with the ductile deformation evidenced by Petford and Atherton (1992). This dextral strike-slip likely corresponds to a late stage of the Quechua 2 tectonic phase (9.5–8.5 Ma) which is characterized by strike-slip movements on NW-SE faults resulting from N-S compression

(Mégard, 1984; Mégard et al., 1984).

Close to the CBNF the ductile deformation recorded NE-SW extension (Fig. 4B). In this area the batholith is young ~4.5 Ma (Stewart et al., 1974; Giovanni, 2007); this NE-SW extension exists at least since the Cordillera Blanca batholith emplacement and is consistent with the initiation of the Callejón de Huaylas subsidence at ~5.4 Ma associated to the CBNF activity (Bonnot, 1984; Giovanni, 2007).

### 5.2. Chronology of the different stress field imprinted in the Cordillera Blanca batholith

The Cordillera Blanca region recorded two steps of ductile deformation and a multistep brittle deformation history. The identified stress fields are: NE-SW extension, N-S extension, E-W compression and ~E-W transtension (Table 1, Figs. 6, 8 and 9). Despite numerous markers of superposed movements on fault planes their relative chronology was unclear. It is not possible to reconstruct the chronology of stress field based on field criteria. Therefore, we compare calculated stress tensor with tectonic phases documented by Mégard (1984) in northern Peru and with the present day stress field inferred from microseismicity (Deverchère et al., 1989).

The ductile deformation indicates a dextral strike-slip at ~8 Ma in the eastern part of the Cordillera Blanca. This deformation could be related to the Quechua 2 period, which has produced dextral
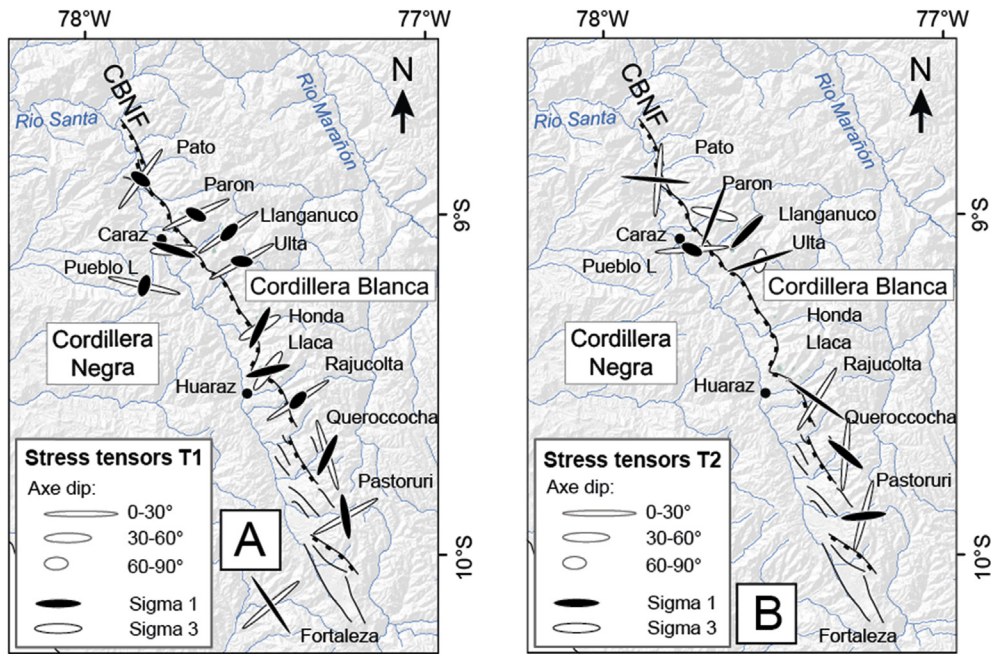
**Fig. 7.** Stress orientation for grouped sites in the Cordillera Blanca region. Stress tensors were calculated using all the fault-slickenline pairs available in one region. Ellipses represents the stress ($\sigma_1$ in black, $\sigma_3$ in white), the direction of the ellipse great axis corresponds to the azimuth of the stress axis; the shape of the ellipse gives the plunge. The two best stress tensors are shown on the maps. A) Stress tensors T1, B) Stress tensors T2.
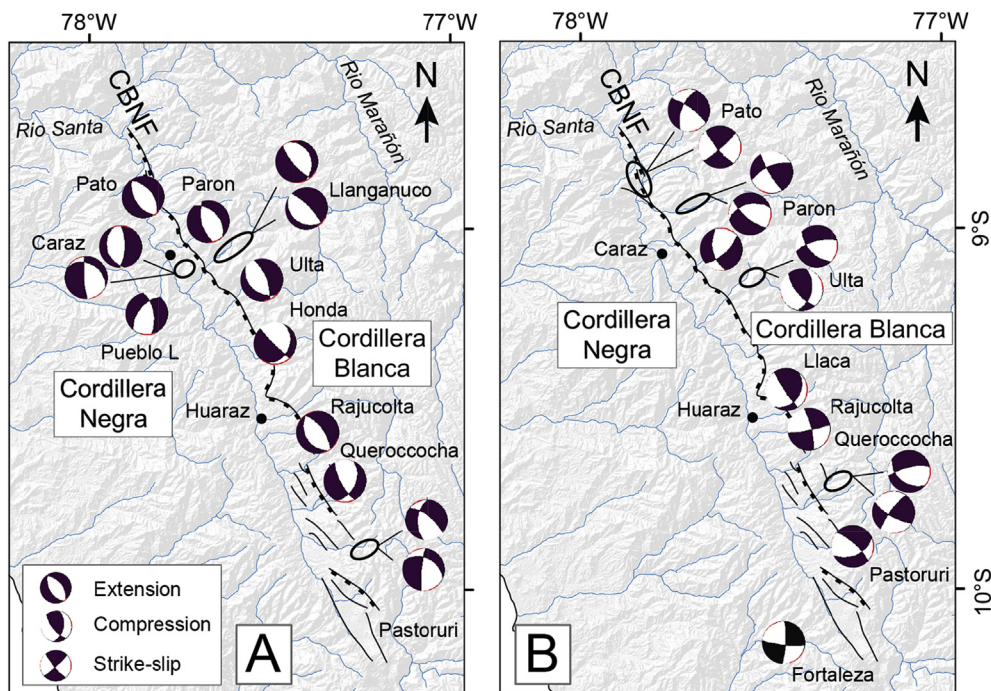


**Fig. 8.** Stress tensors for grouped stations. A) Stress tensors corresponding to the present day regional stress tensor (NE-SW extension) inferred from microearthquakes survey (Deverchère et al., 1989). B) Other stress tensors recorded by the brittle deformation.

strike-slip on NW-SE trending faults in Ayacucho basin between 9.5 and 8.5 Ma (Mégard et al., 1984; Fig. 9). Then, the ductile NE-SW extension observed in the Canyon del Pato (~5 Ma) likely corresponds to the earlier brittle deformation NE-SW extensional tensors. This extension posterior to ~4.5 Ma is in agreement with the initiation of the CBNF at ~5.4 Ma (Bonnot, 1984). Moreover, this NE-SW extension is similar to the regional stress tensor deduced from a

microseismicity survey (Deverchère et al., 1989). Thus, we suggest that these ductile and brittle deformation phases are related to a state of stress identical to state of stress observed at the present day in the Cordillera Blanca region. This state of stress was effective regionally at least for the last ~5 Ma. The extensional stress tensors are not restricted to the Cordillera Blanca. It likely corresponds to a large-scale process driving extension in the overriding plate.
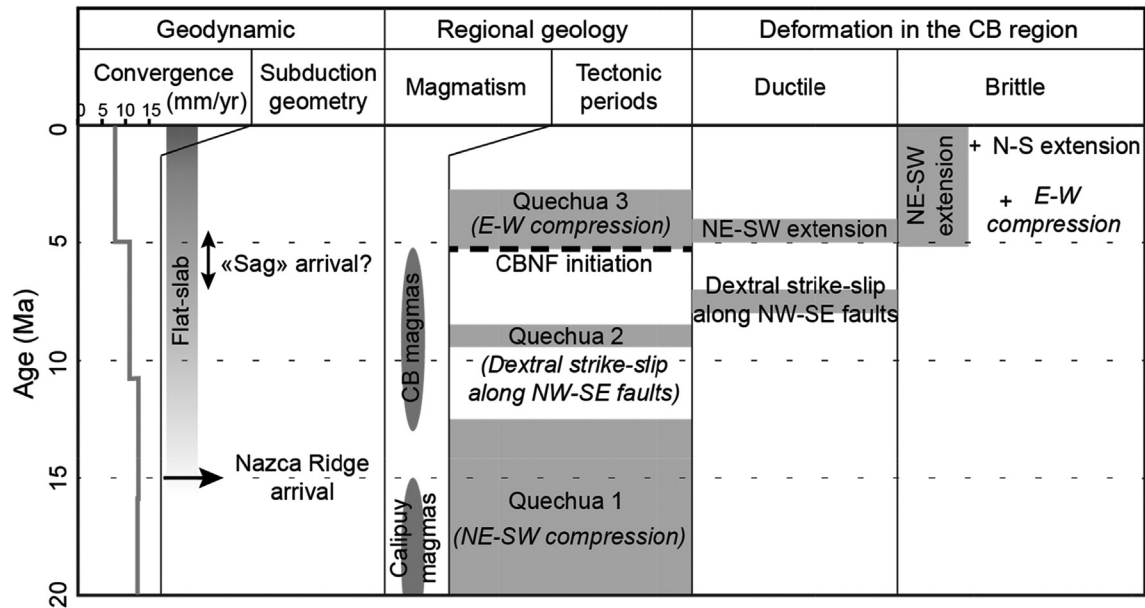
**Fig. 9.** Schematic table that summarizes the northern Peru geodynamic events, regional geology and results of stress field analyzes for the past 20 Ma. The table includes the mean convergence rate (Somoza, 1998), subduction geometry (Barazangi and Isacks, 1976; Gutscher et al., 1999; Rosenbaum et al., 2005; Margirier et al., 2015), magmatism age (e.g., Cobbing et al., 1981; Mukasa, 1984; Beckinsale et al., 1985), tectonic phases (e.g., Mégard, 1984) and our ductile and brittle deformation results.

In addition, the less-expressed stress tensors indicate locally some anomalies in the stress field. Indeed the brittle deformation also indicates that E-W compression episode in the Cordillera Blanca batholith. This compressional episode is also recorded in the Callejón de Huaylas basin (Bonnot, 1984). It could be related to the Pliocene Quechua 3 compressional phase (Mégard, 1984) which could have trigger a brief compressional phase during the CBNF activity (since ~5.4 Ma). Finally, the brittle deformation also recorded multidirectional extension (*Phi* < 0.5) in the Cordillera Blanca (Quebrada Paron, Quebrada Querococha, Quebrada Pastoruri). This stress field could be related to the Quaternary rapid exhumation of the central part of the Cordillera Blanca (Margirier et al., 2016).

### 5.3. Different tectonic phases above the Peruvian flat-slab

This study evidence the occurrence of several tectonic phases above the Peruvian flat-slab segment during the past 8 Myr in agreement with Bonnot (1984) (Fig. 9). These successive tectonic phases and the occurrence of predominant extension perpendicular to the trench suggest that flat-slab segments do not always induce compression in the upper plate as previously suggested (Jordan et al., 1983; Ramos and Folguera, 2009; Martinod et al., 2010). The tectonic regime changes may be associated to other parameters as plates velocities, plates directions, the absolute movement of the trench, the age of the oceanic plate, the presence of sediments or the geometry of the oceanic plate (e.g., Ruff and Kanamori, 1983; Heuret et al., 2007; Schellart, 2008). As the tectonic regime change occurs in a short period of time it could be linked to a local process (versus a large scale geodynamic process). The Peruvian flat slab geometry includes two thickened parts, the Nazca Ridge and the Inca Plateau, and a sag between these two features (Gutscher et al., 1999). Plate reconstructions indicated that the Nazca Ridge subduction initiate at ~10°S at ~15 Ma and then the ridge migrate southward (Hampel, 2002; Rosenbaum et al., 2005; Antonijevic et al., 2015; Fig. 9). The subduction of the Nazca Ridge below the Cordillera Blanca could have induced an increase of the coupling (e.g., Gutscher et al., 2000; McNulty and Farber, 2002;

Martinod et al., 2010) and triggered compressional stress field in this area. After the migration of the ridge toward the South when the sag arrived below the Cordillera Blanca (Fig. 9), the coupling could have decreased and permitted extension in the overriding plate. Indeed, Nocquet et al. (2014) demonstrated that the subduction segments of northern Peru show a low to weak interseismic coupling contrasting with the southern Peru region. Similarly, above the Mexican flat-subduction, Gérault et al. (2015) suggested the control of the mantle dynamic and of a weak subduction interface in the "neutral" state of stress. Finally, all flat slab segments do not trigger extension. For example, no extension have been reported above the Pampean flat-slab in Chile (e.g., Ramos et al., 2002), whereas the Nazca Plate have the same age and dip in these two segments (Barazangi and Isacks, 1976; Müller et al., 2008). The presence of an over-thickened crust (~50 km, James, 1971) in Peru could favor extension independently of subduction properties (Froidevaux and Isacks, 1984). In addition, the amount of sediments on the oceanic plate is different in Peru and Chile: The sediment thickness reaches ~500 m in Peru, in Chile there is no sediments (Divins, 2006). The presence of sediment can change the plate interface properties (Ruff, 1989). Indeed, in Peru GPS survey suggest the subduction interface is not homogeneously coupled along-strike with the existence of a ~500 km-long uncoupled segment in northern Peru whereas in southern Peru and Chile the subduction interface is characterized by highly coupled asperities separated by narrower zones of low interseismic coupling (Nocquet et al., 2014; Saillard et al., 2017).

### 6. Conclusions

Our data suggest a complex tectonic history in the Cordillera Blanca region. The analysis of ductile deformation in the eastern part of the Cordillera Blanca batholith (8 Ma) suggests that the batholith emplaced in a dextral strike-slip context according to Petford and Atherton (1992) observations. In a younger part of the Cordillera Blanca batholith (~4.5 Ma) the ductile deformation indicates NE-SW extension. Then, the multistep deformation recorded in the Cordillera Blanca indicated the succession of different

tectonic regimes (dextral strike-slip, NE-SW extension, E-W compression and NE-SW extension) above the Peruvian flat-slab. The presence of the crustal-scale CBNF and our NE-SW extensional stress tensor suggest that flat subduction can trigger extension in the Western Cordillera while in the Eastern Cordillera the shortening migrate eastward (Mégard, 1984). The extension may be facilitated by the presence of a thickened crust in Peru (Froidevaux and Isacks, 1984), an absolute movement of the overriding plate toward the trench or by a decrease of the convergence rate and a low coupling at the plate interface (Somoza, 1998; Nocquet et al., 2014). In the context of the long-lasting subduction of the Nazca Plate, we suggest that the change of tectonic regime in the overriding plate (from compression to extension) and the extension along the CBNF are likely associated to a decrease of the coupling at the plate interface at the trench and below the Western Cordillera while the shortening migrates eastwards. Finally, considering the occurrence of extension along the CBNF since 5.4 Ma and the predominant NE-SW extension regime, we suggest that flat-slabs do not always favor shortening in the overriding plate. The Peruvian flat-slab seems to not increase the coupling at the trench but only increase the coupling eastward and favor shortening migration in the subandean region.

## Acknowledgments

## Appendix A. Supplementary data

Supplementary data related to this article can be found at http://dx.doi.org/10.1016/j.jsames.2017.04.015.

## References

Angelier, J., 1984. Tectonic analysis of fault slip data sets. J. Geophys. Res. Solid Earth 89 (B7), 5835–5848.

Angelier, J., Mechler, P., 1977. Sur une methode graphique de recherche des contraintes principales également utilisables en tectonique et en séismologie: la méthode des dièdres droits. Bull. la Société Géologique Fr. 19 (6), 1309–1318.

Antonijevic, S.K., Wagner, L.S., Kumar, A., Beck, S.L., Long, M.D., Zandt, G., Tavera, H., Condori, C., 2015. The role of ridges in the formation and longevity of flat slabs. Nature 524 (7564), 212–215. http://dx.doi.org/10.1038/nature14648.

Audin, L., Lacan, P., Tavera, H., Bondoux, F., 2008. Upper plate deformation and seismic barrier in front of Nazca subduction zone: the Chololo Fault System and active tectonics along the Coastal Cordillera, southern Peru. Tectonophysics 459, 174–185. http://dx.doi.org/10.1016/j.tecto.2007.11.070 (1–4) 1.

Barazangi, M., Isacks, B.L., 1976. Spatial distribution of earthquakes and subduction of the Nazca plate beneath South America. Geology 4 (11), 686–692.

Beckinsale, R.D., Sanchez-Fernandez, A.W., Brook, M., Cobbing, E.J., Taylor, W.P., Moore, N.B., 1985. Rb-Sr whole rock isochron and K-Ar determination for the Coastal Batholith of Peru. In: Pitcher, W.S., Atherton, M.P., Cobbing, E.J., Beckinsale, R.D. (Eds.), Magmatism at a Plate Edge: the Peruvian Andes. Blackie Halstead press, Glasgow, pp. 177–202.

Bellier, O., Dumont, J.F., Sébrier, M., Mercier, J.L., 1991. Geological constraints on the kinematics and fault-plane solution of the quiches fault zone reactivated during the 10 November 1946 Ancash earthquake, northern Peru. Bull. Seismol. Soc. Am. 81 (2), 468–490.

Bonnot, D., 1984. Néotectonique et tectonique active de la Cordillère Blanche et du Callejon de Huaylas (Andes nord-péruviennes), Thèse présentée pour obtenir le grade de docteur. Université de Paris-Sud, Centre d'Orsay, pp. 1–202.

Bott, M., 1959. The mechanics of oblique slip faulting. Geol. Mag. 96 (2), 109–117.

Bussel, M.A., Pitcher, W.S., 1985. The structural control of batholith emplacement. In: Pitcher, W.S., Atherton, M.P., Cobbing, E.J., Beckinsale, R.D. (Eds.), Magmatism at a Plate Edge, the Peruvian Andes. Blackie Halstead Press, London, pp. 167–176.

Cobbing, J., Pitcher, W., Baldock, J., Taylor, W., McCourt, W., Snelling, N.J., 1981. Estudio geológico de la Cordillera Occidental del norte del Perú, Instituto Geologico Minero y Metalurgico, Serie D. Estud. Espec. 10 (D), 1–252.

Dalmayrac, B., Molnar, P., 1981. Parallel thrust and normal faulting in Peru and constraints on the state of stress. Earth Planet. Sci. Lett. 55, 473–481.

Delvaux, D. (2012), Release of program Win-Tensor 4.0 for tectonic stress inversion: statistical expression of stress parameters, EGU General Assembly Conference Abstracts.

Delvaux, D., Barth, A., 2010. African stress pattern from formal inversion of focal mechanism data. Tectonophysics 482, 105–128. http://dx.doi.org/10.1016/j.tecto.2009.05.009.

Delvaux, D., and B. Sperner (2003), New aspects of tectonic stress inversion with reference to the TENSOR program, Geological Society, London, Special Publications, 212 (1), 75–100, http://dx.doi.org/10.1144/GSL.SP.2003.212.01.06.

Deverchère, J., Dorbath, C., Dorbath, L., 1989. Extension related to a high topography: results from a microearthquake survey in the Andes of Peru and tectonic implications. Geophys. J. Int. 98 (2), 281–292.

Dewey, J.F., Lamb, S.H., 1992. Active tectonics of the Andes. Tectonophysics 205 (1), 79–95.

Divins, D.L., 2006. Total Sediment Thickness of the World's Oceans and Marginal Seas.

Doser, D.I., 1987. The Ancash, Peru, earthquake of 1946 November 10: evidence for low-angle normal faulting in the high Andes of northern Peru. Geophys. J. R. Astronomical Soc. 91, 57–71.

Farber, D. L., G. S. Hancock (in prep), Tectonic and glacial forcing of motion along an active detachment fault.

Folguera, A., Zapata, T., Ramos, V.A., 2006. Late cenozoic extension and the evolution of the Neuquén Andes. Geol. Soc. Am. Special Pap. 407, 267–285.

Froidevaux, C., Isacks, B.L., 1984. The mechanical state of the lithosphere in the Altiplano-Puna segment of the Andes. Earth Planet. Sci. Lett. 71 (2), 305–314.

Gayet, M., Marshall, L.G., Sempéré, T., 1991. The Mesozoic and Paleocene vertebrates of Bolivia and their stratigraphic context: a review. In: Suárez, R. (Ed.), Fósiles y Facies de Bolivia, vol. 12, pp. 393–433 (3–4).

Gérault, M., Husson, L., Miller, M.S., Humphreys, E.D., 2015. Flat-slab subduction, topography, and mantle dynamics in southwestern Mexico. Tectonics. http://dx.doi.org/10.1002/(ISSN)1944-9194.

Giovanni, M.K., 2007. Tectonic and Thermal Evolution of the Cordillera Blanca Detachment System, Peruvian Andes: Implication for Normal Faulting in a Contractionnal Orogen, 1–255 pp. University of California, Los Angeles.

Giovanni, M.K., Horton, B.K., Garzione, C.N., McNulty, B., Grove, M., 2010. Extensional basin evolution in the Cordillera Blanca, Peru: stratigraphic and isotopic records of detachment faulting and orogenic collapse in the Andean hinterland. Tectonics 29 (6). http://dx.doi.org/10.1029/2010TC002666. TC6007.

Gutscher, M.A., Malavieille, J., Lallemand, S., Collot, J.-Y., 1999. Tectonic segmentation of the north Andean margin: impact of the carnegie ridge collision. Earth Planet. Sci. Lett. 168 (3), 255–270.

Gutscher, M.-A., Spakman, W., Bijwaard, H., Engdahl, E.R., 2000. Geodynamics of flat subduction: seismicity and tomographic constraints from the Andean margin. Tectonics 19 (5), 814–833.

Hampel, A., 2002. The migration history of the Nazca Ridge along the Peruvian active margin: a re-evaluation. Earth Planet. Sci. Lett. 203 (2), 665–679.

Heuret, A., Funiciello, F., Faccenna, C., Lallemand, S., 2007. Plate kinematics, slab shape and back-arc stress: a comparison between laboratory models and current subduction zones. Earth Planet. Sci. Lett. 256 (3), 473–483.

Hodson, K.R., 2012. Morphology, Exhumation, and Holocene Erosion Rates from a Tropical Glaciated Mountain Range: the Cordillera Blanca, Peru, 1–94 pp.. McGill University Masters of science.

Jaillard, E., 1993. L'évolution tectonique de la marge péruvienne au Sénonien et Paleocène et ses relations avec la géodynamique. Bulletin-Société Géologique Fr. 164, 819.

Jaillard, E., 1994. Kimmeridgian to Paleocene tectonic and geodynamic evolution of the Peruvian (and Ecuadorian) margin. In: Salfity, J.A. (Ed.), Cretaceous Tectonics of the Andes. Vieweg, Teubner Verlag, pp. 101–167.

Jaillard, E., Soler, P., 1996. Cretaceous to early Paleogene tectonic evolution of the northern Central Andes (0–18°S) and its relations to geodynamics. Tectonophysics 259 (1), 41–53.

James, D.E., 1971. Plate tectonic model for the evolution of the Central Andes. Geol. Soc. Am. Bull. 82, 3325–3346.

Jordan, T.E., Isacks, B.L., Allmendinger, R.W., Brewer, J.A., Ramos, V.A., Ando, C.J., 1983. Andean tectonics related to geometry of subducted Nazca plate. Geol. Study Am. Bull. 94, 341–361.

Kay, R.W., Kay, S.M., 2002. Andean adakites: three ways to make them. Acta Petrol. Sin. 18 (3), 303–311.

Lacombe, O., 2012. Do fault slip data inversions actually yield "paleostresses" that can be compared with contemporary stresses? A critical discussion. Comptes Rendus Geosci. 344 (3–4), 159–173. http://dx.doi.org/10.1016/j.crte.2012.01.006.

Margirier, A., Robert, X., Audin, L., Gautheron, C., Bernet, M., Hall, S., Simon-Labric, T., 2015. Slab flattening, magmatism and surface uplift in the Cordillera Occidental (northern Peru). Geology 1–4. http://dx.doi.org/10.1130/G37061.1.

Margirier, A., Audin, L., Robert, X., Herman, F., Ganne, J., Schwartz, S., 2016. Time and mode of exhumation of the Cordillera Blanca batholith (Peruvian Andes). J. Geophys. Res. Solid Earth 121. http://dx.doi.org/10.1002/2016JB013055.

Marrett, R., Allmendinger, R.W., 1990. Kinematic analysis of fault-slip data. J. Struct. Geol. 12 (8), 973–986.

Martinod, J., Husson, L., Roperch, P., Guillaume, B., Espurt, N., 2010. Horizontal subduction zones, convergence velocity and the building of the Andes. Earth Planet. Sci. Lett. 299 (3–4), 299–309. http://dx.doi.org/10.1016/

j.epsl.2010.09.010.

McKee, E.H., Noble, D.C., 1982. Miocene volcanism and deformation in the western Cordillera and high plateaus of south-central Peru. Geol. Soc. Am. Bull. 93 (8), 657–662.

McNulty, B.A., Farber, D.L., 2002. Active detachment faulting above the Peruvian flat slab. Geology 30 (6), 567–570.

McNulty, B.A., Farber, D.L., Wallace, G.S., Lopez, R., Palacios, O., 1998. Role of plate kinematics and plate-slip-vector partitioning in continental magmatic arcs: evidence from the Cordillera Blanca, Peru. Geology 26 (9), 827–830.

Mégard, F., 1978. Etude géologique des Andes du Pérou central: Mémoire ORSTROM, p. 86.

Mégard, F., 1984. The Andean orogenic period and its major structures in central and northern Peru. J. Geol. Soc. 141 (5), 893–900.

Mégard, F., Noble, D.C., McKEE, E.H., Bellon, H., 1984. Multiple pulses of Neogene compressive deformation in the Ayacucho intermontane basin, Andes of central Peru. Geol. Soc. Am. Bull. 95 (9), 1108–1117.

Mukasa, S.B., 1984. Comparative Pb Isotope Systematics and Zircon U-Pb Geochronology for the Coastal, San Nicolás and Cordillera Blanca Batholiths, Peru. PhD thesis. University of California, Santa Barbara.

Müller, R.D., Sdrolias, M., Gaina, C., Roest, W.R., 2008. Age, spreading rates, and spreading asymmetry of the world's ocean crust. Geochem. Geophys. Geosyst. 9 (4), 1–19. http://dx.doi.org/10.1029/2007GC001743.

Noble, D.C., McKee, E.H., Mourier, T., Mégard, F., 1990. Cenozoic stratigraphy, magmatic activity, compressive deformation, and uplift in northern Peru. Geol. Soc. Am. Bull. 102 (8), 1105–1113.

Nocquet, J.-M., et al., 2014. Motion of continental slivers and creeping subduction in the northern Andes. Nat. Geosci. 7 (4), 287–291. http://dx.doi.org/10.1038/ngeo2099.

Ortner, H., Reiter, F., Acs, P., 2002. Easy handling of tectonic data: the programs TectonicVB for Mac and TectonicsFP for Windows™. Comput. Geosciences 28 (10), 1193–1200.

Pardo-Casas, F., Molnar, P., 1987. Relative motion of the Nazca (Farallon) and South American plates since late cretaceous time. Tectonics 6 (3), 233–248.

Petford, N., Atherton, M.P., 1992. Granitoid emplacement and deformation along a major crustal lineament: the Cordillera Blanca, Peru. Tectonophysics 205 (1), 171–185.

Pêcher, A., et al., 2008. Stress field evolution in the northwest Himalayan syntaxis, northern Pakistan. Tectonics 27 (6). http://dx.doi.org/10.1029/2007TC002252. TC6005.

Ramos, V.A., Folguera, A., 2009. Andean flat-slab subduction through time. Geol. Soc. Lond. Spec. Publ. 327 (1), 31–54. http://dx.doi.org/10.1144/SP327.3.

Ramos, V.A., Cristallini, E.O., Pérez, D.J., 2002. The Pampean flat-slab of the central Andes. J. S. Am. Earth Sci. 15 (1), 59–78.

Rosenbaum, G., Giles, D., Saxon, M., Betts, P.G., Weinberg, R.F., Duboz, C., 2005. Subduction of the Nazca Ridge and the Inca Plateau: insights into the formation of ore deposits in Peru. Earth Planet. Sci. Lett. 239 (1–2), 18–32. http://dx.doi.org/10.1016/j.epsl.2005.08.003.

Ruff, L.J., 1989. Do trench sediments affect great earthquake occurrence in subduction zones? Subduction Zones Part II 129 (1–2), 264–282.

Ruff, L.J., Kanamori, H., 1983. Seismic coupling and uncoupling at subduction zones. Tectonophysics 99 (2–4), 99–117.

Saillard, M., Audin, L., Rousset, B., Avouac, J.P., Chlieh, M., Hall, S.R., Husson, L., Farber, D.L., 2017. From the seismic cycle to long-term deformation: linking seismic coupling and Quaternary coastal geomorphology along the Andean megathrust. Tectonics 36 (2), 241–256. http://dx.doi.org/10.1029/2002JB002072.

Schellart, W.P., 2008. Overriding plate shortening and extension above subduction zones: a parametric study to explain formation of the Andes Mountains. Geol. Soc. Am. Bull. 120 (11–12), 1441–1454.

Scheuber, E., Gonzalez, G., 1999. Tectonics of the Jurassic- Early Cretaceous magmatic arc of the north Chilean Coastal Cordillera (22°-26°S): a story of crustal deformation along a convergent plate boundary. Tectonics 18 (5), 895–910.

Schwartz, D.P., 1988. Paleoseismicity and neotectonics of the Cordillera Blanca fault zone, northern Peruvian Andes. J. Geophys. Res. 93 (B5), 4712–4730.

Sébrier, M., Mercier, J.L., Macharé, J., Bonnot, D., Cabrera, J., Blanc, J.L., 1988. The state of stress in an overriding plate situated above a flat slab: the Andes of Central Peru. Tectonics 7 (4), 895–928.

Siame, L.L., Sébrier, M., Bellier, O., Bourles, D., 2006. Can cosmic ray exposure dating reveal the normal faulting activity of the Cordillera Blanca Fault, Peru? Rev. la Asoc. Geol. Argent. 61 (4), 536–544.

Silgado, E. F. (1992), Investigaciones de sismicidad histórica en la América del Sur en los siglos XVI, XVII, XVIII y XIX, Consejo Nacional de Ciencia y Tecnología, Lima.

Somoza, R., 1998. Updated Nazca (Farallon)—south America relative motions during the last 40 My: implications for mountain building in the central Andean region. J. S. Am. Earth Sci. 11 (3), 211–215.

Soulas, J.P., 1977. Las fases tectonicas del Terciario Superior en Peru-corte Ayacucho-Pisco. Bol. Soc. Geol. del Perú 57–58.

Sperner, B., Ratschbacher, L., Ott, R., 1993. Fault-striae analysis: a Turbo Pascal program package for graphical presentation and reduced stress tensor calculation. Comput. Geosciences 19 (9), 1361–1388.

Steinmann, G., 1929. Geologie von Peru. In: Winter, K. (Ed.), Heidelberg, p. 448.

Stewart, J.W., Evernden, J.F., Snelling, N.J., 1974. Age determinations from Andean Peru: a reconnaissance survey. Geol. Soc. Am. Bull. 85 (7), 1107–1116.

Taylor, G.K., Grocott, J., Pope, A., Randall, D.E., 1998. Mesozoic fault systems, deformation and fault block rotation in the Andean forearc: a crustal scale strike-slip duplex in the Coastal Cordillera of northern Chile. Tectonophysics 299 (1), 93–109.

Wallace, R.E., 1951. Geometry of shearing stress and relation to faulting. J. Geol. 118–130.

Wipf, M. (2006), Evolution of the Western Cordillera and Coastal Margin of Peru: Evidence from low-temperature Thermochronology and Geomorphology, 1–163 p. Swiss Federal Institute of Technology Zürich, 7 March.

Wise, J.M., Noble, D.C., 2003. Geomorphic evolution of the Cordillera Blanca, northern Peru. Bol. la Soc. Geol. del Peru 96, 1–21.

Yamaji, A., 2000. The multiple inverse method: a new technique to separate stresses from heterogeneous fault-slip data. J. Struct. Geol. 22 (4), 441–452. http://dx.doi.org/10.1016/S0191-8141(99)00163-7.

Zeilinger, G., Burg, J.P., Chaudhry, N., Dawood, H., Hussain, S., 2000. Fault systems and Paleo-stress tensors in the Indus suture Zone (NW Pakistan). J. Asian Earth Sci. 18, 547–559.